3-HAA Metabolic Pathway Regulates HCC Growth

Zhaopeng Shi
Shanghai Jiao Tong University School of Medicine
Guifang Gan
Shanghai Jiao Tong University School of Medicine
Xianfu Gao
Shanghai Jiao Tong University School of Medicine
Fuxiang Chen
Shanghai Jiao Tong University School of Medicine
Jun Mi (jmei@sjtu.edu.cn)
Shanghai Jiao Tong University School of Medicine

Research

Keywords: 3-hydroxyanthronic acid (3-HAA), DUSP6, Hepatocellular Carcinoma (HCC)

Posted Date: September 21st, 2021

DOI: https://doi.org/10.21203/rs.3.rs-898525/v1

Abstract

Background

Kynurenine, a metabolite of tryptophan, promotes immune tolerance in development and tumor evasion by binding to the aryl hydrocarbon receptor (AHR). However, the kynurenine catabolic enzyme IDO1 inhibitors fail in clinical trials.

Methods

The LC-MS/MS and GC-MS/MS were performed to measure the concentration of tryptophan metabolites. The PCX model, PDX model, and transposon liver cancer models were used to evaluate the effects of 3-HAA, DUSP6, and YY1 on HCC tumor formation and/or tumor growth.

Results

3-hydroxyanthranilic acid (3-HAA) induced HCC apoptosis and reduced xenografted tumor growth, the survival of the transposon HCC mice, and synergized with IDO1 inhibitor on HCC growth *in vivo*. Overexpression of 3-HAA synthesis enzyme KMO suppressed tumor formation and tumor growth by increasing endogenous 3-HAA while adding exogenous 3-HAA also inhibited tumor growth. Notably, 3-HAA was lower in tumor cells due to the downregulation of its synthetic enzyme KMO/KYNU and/or upregulation of its catalytic enzyme HAAO. The mechanistic investigation demonstrated that 3-HAA induced dual-specificity phosphatase 6 (DUSP6) transcription. DUSP6 overexpression induced apoptosis of hepatocellular carcinoma (HCC) cells and suppressed the HCC growth *in vitro* and *in vivo*. DUSP6 knockdown abolished 3-HAA-induced apoptosis and restores tumor growth.

Conclusions

These findings demonstrate that 3-HAA metabolic pathway regulates HCC cell growth, suggesting it is a promising therapeutic candidate for HCC.

Background

The essential amino acid tryptophan is catabolized mainly through the serotonin pathway in the gut and the brain and through the kynurenine pathway in the liver [1, 2]. Tryptophan metabolism is enhanced in various tumors by upregulating the indoleamine 2,3-dioxygenase 1/2 (IDO1/2) or tryptophan 2,3-dioxygenase (TDO2), the rate-limiting enzymes in the kynurenine metabolism pathway [3–5]. TDO2 is the main enzyme generating kynurenine in hepatocytes [6]. Kynurenine, a catabolite of tryptophan, increases immune tolerance in development and disease by directly binding to the aryl hydrocarbon receptor (AHR) [7, 8]. Kynurenine is believed to promote tumor growth by enhancing tumor immune evasion [7] [9] [10].

The 3-hydroxyanthranilic acid (3-HAA), a derivative of kynurenine, was reported to exert anti-inflammatory effects by selectively inducing the apoptosis of activated T cells [11, 12]. However, the function of other kynurenine derivatives largely remains unclear. Here, we report 3-HAA, selectively decreased in various tumors, regulates transcription factor YY1 and consequently induces tumor cell apoptosis and suppresses HCC growth *in vitro* and *in vivo*.

Methods

Cells

Human HCC cell line HepG2 (American Type Culture Collection; Manassas, VA, USA; RRID: CVCL_0027), Hep3B (RRID: CVCL_0326), PLC8024 (RRID: CVCL_0485) (Cell Bank of the Chinese Academy of Science, Shanghai, China), MHCC97L (RRID: CVCL_4973), MHCC97H (RRID: CVCL_4972), Huh7 (RRID: CVCL_0336), LO2 (RRID: CVCL_6926), WRL68(RRID: CVCL_0581) and SMMC7721 (RRID: CVCL_0336) (Genechem Co., Ltd., Shanghai, China) were grown at 37°C in DMEM (Invitrogen, Grand Island, NY, USA) containing 5% CO_2 atmosphere and supplemented with 10% heat-inactivated fetal bovine serum (PAA, Australia) in the presence of 100 U/mL penicillin and 0.1 mg/mL streptomycin.

Plasmids

The pGIPZ-shHAAO-1, pGIPZ-shHAAO-2, pGIPZ-shHAAO-3, pGIPZ-shDUSP6-1, pGIPZ-shDUSP6-2, pGIPZ-shYY1-1 and pGIPZ-shYY1-2 were purchased from SHSMU DNA Library. The pTSB-KMO was purchased from Genewiz. pLenti-HA-YY1-WT was constructed by PCR using primers WT-F: CCGGAATTCATGTACCCATACGACGTCCCAGACTACGCTGCCTCGGGCGACAC and WT-R: CGCGGATCCTCACTGGTTGTTTTTGGCCTTAGC. The YY1-T398A and YY1-T398E mutant vectors are obtained using mutagenesis kit (TOYOBO, cat: SMK-101) and primers YY1-F-T398E: gtttgctcagtcaGAAaacctgaaatctcacatc, YY1-F-T398A: gtttgctcagtcaGCAaacctgaaatctcacatc and YY1-R-mut: ttcttattacaaccatcgaaggggcacac. For the construction of pET-28a(+)-YY1, a BamHI/EcoRI fragment encompassing the CDS of human YY1 (NM_003403.4) was amplified from human cDNA by PCR using primers YY1-F: CGGGATCCATGGCCTCGGGCGACACCC and YY1-R: CCGGAATTCTCACTGGT TGTTTTTGGCCTTAGCA, and the fragment was inserted into pET28a(+) vector for bacterial expression.

Colony formation

HCC cells were seeded into 6-well dishes at a cell density of 1000 cells/well and treated with drugs for 10–14 days until clones were visible. PBS-washed cells were fixed with 4% paraformaldehyde and stained with 1% crystal violet. The stained clones were counted.

Cell proliferation assay

Cell proliferation was measured using the Cell Counting Kit-8 reagent (CCK-8, Dojindo, cat: CK04). HCC cells were seeded into a 96-well plate at 2000 cells/well, were treated with 3-HAA (Sigma, cat: 148776) and ZVAD (TargetMol, cat: T6013) at appropriate doses as indicated in the figure legend. CCK-8 assays

were performed in triplicates as instructed by the manufacturer for 2 hours at indicated time points. Absorbance was measured at 450 nm using a microplate reader, and cell viability was normalized to control, and the mean of at least three independent experiments was calculated.

Flow cytometry

HCC cells were treated with 3-HAA at appropriate doses for 48 hours and harvested by trypsinization and washed with phosphate-buffered saline (PBS). The cells were then stained with anti-human Annexin V-APC and PI-PE (Multisciences Inc, cat: AP107-100) for 30 min. At least 1 x 10^6 cells were analyzed by a FACS Aria II (BD Falcon, Franklin Lakes, NJ, USA). Cells were gated based on their forward and side scatter properties. Furthermore, mouse xenograft tissues were minced and digested with collagenase and DNase Ⅰ (Transgen, GD201-01) at 37°C for 30 min and then filtered with 40-micron cell strainers (BD Falcon). Tumor cells were stained with annexin-V/propidium and analyzed by flow cytometry.

ChIP analysis

Chromatin was isolated from HCC cells treated with or without 3-HAA and fragmented to a size range from 150 to 400 bp. The solubilized chromatin fragments were immunoprecipitated with antibodies against YY1 (Active Motif, cat: 61779). The recovered DNA fragments were processed for DNA sequencing by the Illumina Genome Analyzer. The generated short reads were mapped onto the genome, and the peak calling program was used to identify peaks with the mapped reads.

For ChIP-PCR and ChIP-QPCR, primers (ChIP-NC-F: CACCTGCTTAGCACAGTTTCCA, ChIP-NC-R: GTCCAGCAAAACCTGATGGATT, ChIP-DUSP6-F: CCTCCATCCGGCTTCCAAT, ChIP-DUSP6-R： GGTAACTTTGGGGAGGTGCG, ChIP-PC-F： GACAGGTCTGAAGCCTGGAG, ChIP-PC-R: CGGGACGTGAAAGGTTAGAA) were used to detect the accumulation of YY1 in the DUSP6 promoter.

Western blotting assays

Appropriate cells were lyzed in RIPA lysis buffer containing a cocktail of protease inhibitors (Roche) and PMSF. Total protein concentration was determined using the bicinchoninic acid (BCA) assay kit (Ding Guo Biotechnology, cat: BCA02). For nuclear and cytoplasmic protein analysis, the Nuclear and Cytoplasmic Protein Extraction Kit (Beyotime, cat: P0028) was used according to the instructions. For immunoprecipitation, HCC cells were lyzed in lysis buffer (50mM Tris, 150mM NaCl, 1% TritonX-100, and 1mM EDTA) containing a cocktail of protease inhibitors and PMSF. Protein A/G beads, HA/YY1 antibodies were added to soluble protein and incubated overnight at 4℃, with gentle agitation. Immunoprecipitated materials were washed three times, eluted with loading buffer at 95℃ for 5 min, and analyzed by western blotting. Antibodies against the following proteins were used for immunoblotting: IDO1 (CST, cat: 86630), TDO2 (Origene, cat: TA504879), KYNU (Proteintech, cat: 11796-1-AP), KMO (Proteintech, cat: 10698-1-AP), HAAO (Proteintech, cat: 12791-1-AP), Cleaved Caspase3 (CST, cat:9315), PARP (Proteintech, cat: 13371-1-AP), DUSP6 (Proteintech, cat: 10433-1-AP), IGFBP1 (Proteintech, cat: 13981-1-AP), p-ERK (CST, cat: 4370), ERK (CST, cat: 4695), BAD (CST, cat: 9239), BCL2 (CST, cat: 4223), BCL-XL (CST, cat: 2764), YY1 (Active Motif, cat: 61779), H3 (Proteintech, cat: 17168-1-AP), p-YY1

(Abclonal, cat: E13449), HA (Sangon, cat: D110004), PKCζ (CST, cat: 9368), RIP3 (Proteintech, cat: 17563-1-AP), P62 (CST, cat: 5114), LC3B (CST, cat: 2775), CYP1A1 (Proteintech, cat: 13241-1-AP), CYP1B1 (Proteintech, cat: 18505-1-AP), TIPARP (Sigma, cat:SAB2102431) and β-actin (Santa Cruz, cat: 47778). The immunoblots were scanned using an Odyssey infrared imaging system (LI-COR). Immunolabeling was detected using the ECL reagent (Sigma). Protein expression was normalized against β-actin.

Real-time quantitative PCR

Total cellular RNA was prepared using the TRIzol reagent (Invitrogen, cat: 15596018) as instructed by the manufacturer and was reverse transcribed using a reverse transcription reagent kit (TAKARA, cat: RR036A). After cDNA synthesis, real-time quantitative polymerase chain reaction (PCR) was performed in triplicate in a 96-well plate with an ABI7500 real-time PCR system (Life Technologies, Grand Island, NY, USA) using SYBR Green mixture (AG, cat: AG11702). CYP1A1, CYP1B1, and TIPARP expression were normalized against β-actin. The primer sequences were as follows: *IGFBP1*-F 5'-GGCTCTCCATGTCACCAACA – 3', *IGFBP1*-R 5'- CCATTCCAAGGGTAGACGCA – 3', *DUSP6*-F 5'-CCTGCATTGCGAGACCAATC – 3', *DUSP6*-R 5'- GGGGGTGACGTTCAAGATGT – 3', *NR0B2*-F 5'-GCCTGAAAGGGACCATCCTC – 3', *NR0B2*-R 5'- CCAGGGTTCCAGGACTTCAC – 3', *EGLN3*-F 5'-CTTTGTGGCCTTCTTTGA AGT – 3', *EGLN3*-R 5'- CCACACAGTTGCTCCACAT – 3', *PFKFB4*-F 5'-GGATCCCGGACCTCGATTCT – 3', *PFKFB4*-R 5'- CCCAGGAAGTTGTCCAGGTAG – 3', *IER3*-F 5'-AAGCCCATCCACCGCTAAAA – 3', *IER3*-R 5'- AGAAGCCTTTTGGCTGGGTT – 3', *CYP1A1*-F 5'-TCGGCCACGGAGTTTCTTC – 3', *CYP1A1*-R 5'- GGTCAGCATGTGCCCAATCA-3', *CYP1B1*-F 5'-TGAGTGCCGTGTGTTTCGG-3', *CYP1B1*-R 5'- GTTGCTGAAGTTGCGGTTGAG-3', *TIPARP*-F 5'-AGAACGAGTGGTTCCAATCCA-3', *TIPARP-R* 5'- TGGGTGCAAAAGATCAGTCTG-3', *β-actin*-F 5'-GCGGGAAATCGTGCGTGACATT-3' and *β-actin*-R 5'-GATGGAGTTGAAGGTAGTTTCG-3'.

Immunohistochemistry

Tissue samples were fixed in 4% paraformaldehyde (PFA) and embedded in paraffin. Primary antibodies used were 3-HAA (Abcam, ab15580), KYNU (Proteintech, cat: 11796-1-AP), KMO (Proteintech, cat: 10698-1-AP), HAAO (Proteintech, cat: 12791-1-AP), IDO1 (CST, cat: 86630), and DUSP6 (Proteintech, cat: 10433-1-AP). Detection was performed with the Elivision super Kit (MXB, cat: KIT-9921) and DAB Substrate (Boster, cat: AR1022), followed by hematoxylin counterstaining (BBI, cat: E607317).

Electrophoretic mobility shift assay

Promoter fragments were generated by primers (DUSP6-1145-1134-F: ACGCCTCCATCCGGCTTCCA, DUSP-1145-1134-R: TGGAAGCCGGATGGAGGCGT, DUSP6-1145-1134-F-mut: ACGCCTCCATCCGGCTTCCA, DUSP-1145-1134-R-mut: TGGAAGCCGGATGGAGGCGT), before labeling at 5' terminal of the primers using FAM. Promoter fragments were incubated with YY1 in ASSAY BUFFER (Tris-HCl 20mM, NaCl 100mM, $MgCl_2$ 1mM, DTT 1mM and Glycerol 4%, pH = 8.0) for 20min at 37℃, and separated by polyacrylamide gel electrophoresis.

Dual-luciferase reporter

For luciferase assay, the promoter region of human DUSP6 was moved from pGL2-DUSP6 (a gift from Dr. Norton, University of Florida) by digestion, gel purified, and inserted into a KpnI/XhoI digested pGL4 vector. We constructed some mutants using primers (DUSP6-promoter-F: GGGGTACCCGAACACGCTCCTCCAGG, DUSP6-promoter-R: CCCTCGAGCGGCCGCCAGTGTGAT, DUSP6-F1-m-1598-1587: TGGCAACCTAGGCCTCGCAAAATTTCCCGGGTAGCCTACATTTCCCAAACCAG, DUSP6-R1-m-1598-1587: GGTTTGGGAAATGTAGGCTACCCGGGAAATTTTGCGAGGCCTAGGTTGCCA, DUSP6-F1-m-1145-1134: GGCCCCCACCCGGCCACGCCCTTCCTTTTTCCCCAATCCGTCCGCCCCGCGG and DUSP6-R1-m-1145-1134: GCCGCGGGGCGGACGGATTGGGGAAAAAGGAAGGGCGTGGCCGGGTGGGGGCC).

293T cells were co-transfected with 100ng different pGL4-DUSP6-promoter vectors, 800ng pSG5-YY1, or pSG5, and 1 ng pRL-TK-Renilla luciferase plasmids. After 48 hours, the cells were lysed, and luciferase activity was measured using the Dual-Luciferase Reporter Assay System (Promega) according to the manufacturer's instructions.

RNA-Seq

RNA was extracted from HCC cells with the TRIzol reagent (Invitrogen, cat: 15596018) according to the instructions. RNA-seq libraries were prepared with the Ovation RNASeq Systems 1–16 (Nugen), and indexed libraries were multiplexed in a single flow cell and underwent 75 base pair single-end sequencing on an Illumina NextSeq500 using the High Output kit v2 (75 cycles) at BGI Group.

Lentivirus Production

293T cells were cultured in DMEM supplemented with 10% fetal bovine serum (Gibco) and were maintained at 37℃ in a humidified atmosphere with 5% CO_2. For virus production, 8 μg of the appropriate plasmid and 3.2 mg of helper plasmids (2μg pMD2.G and 6μg psPAX2) were transfected into 293T cells cultured at 80% confluence in a 10 cm dish using Lipoplus (SAGE) according to the manufacturer's instructions. Viral supernatants were collected 48 hours after transfection and filtered through a 0.45 mm filter.

Silver Stain

HCC cells were treated with 100μM of 3-HAA for 24 hours. Cells were collected and lysed by lysis buffer. Proteins were separated by SDS-PAGE and stained by using Fast Silver Stain Kit (Beyotime, cat: P0017S) according to the instructions.

Metabolism flux analysis by LC-MS/MS

For the flux experiment of tryptophan catabolism, tryptophan in the medium was replaced by fully ^{13}C-labeled tryptophan (tryptophan-$^{13}C_{11}$). Sample preparation and LC-MS/MS analysis were the same as for quantitation of tryptophan catabolic products, except that the parameters of MRM transitions were different. MRM transitions for catabolic products of tryptophan-$^{13}C_{11}$ (M11: 320 > 273) were set as 5-hydroxyindoleacetic acid (M10: 323 > 155), kynurenine (M10: 427 > 122), kynurenic acid (M10: 304 > 105), 3-hydroxykynurenine (M10: 547 > 05), xanthurenic acid (M10: 424 > 05), 3-hydroxyanthranilic acid (M7:

369 > 247), cinnabarinic acid (M14: 419 > 105). Simultaneously, the MRM transitions (M0) of unlabeled tryptophan and its catabolic products were acquired using the same settings as in quantitation experiments.

Quantitative proteomics

Cell samples were sonicated three times on ice using a high-intensity ultrasonic processor (Scientz, Ninbo, Zhejiang, China) in lysis buffer (8 M urea, 1% Protease Inhibitor Cocktail). The supernatant was collected, and proteins were reduced with five mM dithiothreitol for 30 min at 56°C, then alkylated with 11 mM iodoacetamide for 15 min at room temperature in darkness. Following the addition of 100 mM TEAB to dilute the urea to < 2 M, trypsin was added to the protein samples first at a trypsin-to-protein mass ratio of 1:50 for digestion overnight, then at a ratio of 1:100 for second digestion lasting four h.

After trypsin digestion, peptides were desalted on a Strata X C18 SPE column (Phenomenex) and vacuum-dried. Peptides were reconstituted in 0.5 M TEAB and processed according to the manufacturer's protocol for the TMT kit/iTRAQ kit. The tryptic peptides dissolved in 0.1% formic acid (solvent A) were directly loaded onto a custom-made reverse-phase analytical column (15-cm length, 75 μm i.d.) on an EASY-nLC 1000 UPLC system. The gradient to solvent B (0.1% formic acid in 98% acetonitrile) increased from 6–23% over 26 min, then from 23–35% in 8 min and then to 80% in 3 min, after which it remained at 80% for 3 min. The flow rate was constant at 400 nL/min.

Peptides were subjected to NSI source followed by tandem mass spectrometry (MS/MS) in Orbitrap Fusion™ Tribrid™ (Thermo, CA, USA) coupled online to the UPLC. Intact peptides were detected in the Orbitrap at a resolution of 60,000. Peptides were selected for MS/MS by NCE at 35; ion fragments were detected in the Orbitrap at a resolution of 30,000. A data-dependent procedure that alternated between one MS scan followed by 10 MS/MS scans was applied for the top 10 precursor ions above a threshold intensity, which were greater than 5×10^3 in the MS survey scan with dynamic exclusion of 30.0 s. The electrospray voltage applied was 2.0 kV. Automatic gain control was used to prevent the orbitrap from overfilling; 5×10^4 ions were accumulated to generate MS/MS spectra. For MS scans, the *m/z* scan range was from 350 to 1550. The fixed first mass was set as 100 *m/z*. MS/MS data were processed using the Maxquant search engine (version 1.5.2.8). Carbamidomethyl on cysteine was specified as a fixed modification, while oxidation on methionine was specified as a variable modification. FDR was adjusted to < 1% and the minimum score for peptides was set to > 40.

TUNEL assay

The cover glass was placed in the 24-well plate, and the HCC cells were inoculated on the cover glass overnight. DMSO or 100 μM 3-HAA was added to the culture medium for 48 hours. The cells were washed with PBS for three times. Add 0.5mL of 4% paraformaldehyde and fix cells at room temperature for 10 minutes. Cells were treated with 0.4%Triton X-100 for 5 minutes and washed with PBS. Cells on the cover glass were treated with TUNEL staining solution and incubated in a wet box at 37℃ for 1 hour. DAPI

staining solution was used to stain the nuclear for 5 minutes in dark. Cells were observed and photographed under a fluorescence microscope.

HCC-PCX mouse model

Six-week-old male BALB/c nude mice or male immune-competent C57BL/6 mice were purchased from Lingchang, Shanghai, China. Xenograft mouse model of HCC was generated by injecting SMMC-7721 HCC cells (1.5×10^6) or mouse live cancer Hep1-6 cells (1 × 10^6) subcutaneously into the armpit of the rear limb. These SMMC-7721 cells were overexpressing KMO or T398E/T398A mutant YY1 or depleted of HAAO, DUSP6, or YY1. Mice were injected intraperitoneally with 100 mg/kg of 3-HAA or an equal amount of DMSO every day. The PKC inhibitor Go6983 was injected intravenously every two days. The dose of Go6983 was 0.8 mg/kg.day, and the IDO1 inhibitor Epacadostat was orally administered at the dose of 100 mg/kg.day.

After two weeks, subcutaneously transplanted tumors were removed, and the volume was measured, and the tumors were photographed. Following homogenization or tissue slicing, the flow cytometry analysis and TUNEL assay were performed to determine the ratio of apoptotic cells in xenografts. For flow cytometry analysis, cells were collected in binding buffer and stained with Annexin V-APC and PI, and apoptotic signals were detected by flow cytometry.

HCC-PDX mouse models

This study received ethics board approval at the Shanghai Jiao Tong University School of Medicine. The HCC-PDX models (LIV#031, #046, and #057) were initially isolated from patients and were stored in liquid nitrogen. Mice were maintained under specific-pathogen-free (SPF) conditions. Once the recovered tumors grew to 250 mm^3 in mice, tumor tissues were cut into 2×2 mm pieces and implanted subcutaneously into SCID mice [24]. The 3-HAA were intraperitoneally administered every day when the tumor volume reached approximately 200 mm^3. Tumor size and mice body weight were monitored for up to 4 weeks, and tumor volume (TV) was calculated.

Transposon HCC mouse Model

This induced HCC mouse model was adopted from the literature [25–27]. Briefly, HCC inducing oncogenes β-Catenin and MET in pT2 vector along with Sleeping Beauty transposon (SB100) was introduced with GFP, pT2-shDUSP6, or pT2-shYY1 (also in pT2 vector) into C57BL/6 mice. Thirty micrograms of the oncogene plasmids and three micrograms SB100 plasmids were diluted in 2 ml of a filtered 0.9% NaCl solution and followed by an injection into the lateral tail veins of 6-week-old mice. Livers of some mice were harvested to determine tumor burden at a specific time after hydrodynamic transfection (HDT). The six mice in each group were used for survival analysis.

Statistical analysis

Data were presented as means ± SD. All data were representative of at least three independent experiments. The unpaired two-tailed Student's *t*-test and the Two-way ANOVA were used as indicated. All

presented differences were $P < 0.05$ unless otherwise stated.

Results

3-HAA is decreased in tumor cells

To comprehensively understand the effect of kynurenine derivatives on tumors, tryptophan catabolites were first analyzed in clinical HCCs using liquid chromatography-tandem mass spectrometry (LC-MS/MS) and gas chromatography-mass spectrometry (GC-MS). The concentration of kynurenine catabolite 3-HAA decreased in 37 cases of HCC ($p < 0.01$) and 42 cases of esophageal carcinomas ($p < 0.01$) compared to the matched paratumor tissues (Figs. 1A and S1A). Conversely, the concentration of tryptophan and kynurenine was higher in these HCCs and esophageal carcinomas than in the matched paratumor tissues, respectively. There was no significant difference in 3-hydroxykynurenine (3-HK) between tumors and adjacent non-cancerous tissues. Consistent with this observation, the concentration of 3-HAA was also lower in seven HCC cell lines tested than in normal hepatic LO2 cells, whereas the content of tryptophan and kynurenine increased in these tested HCC cell lines (Fig. 1B). The immunohistochemistry analysis further confirmed lower 3-HAA content in clinical HCC tissues than in adjacent non-cancerous tissues (Fig. 1C).

Metabolic flux analysis revealed tryptophan metabolized to kynurenine but not 3-HK or 3-HAA in HCC cells, and the newly generated kynurenine was secreted into the culture medium (Fig. 1D), suggesting 3-HAA is decreased in tumors, at least in HCCs and esophageal carcinomas.

Upregulation of KMO increases 3-HAA

To determine whether the metabolic enzymes regulate 3-HAA concentration, we assessed the expression of 3-HAA-related enzymes in HCC cells. The immunoblotting and immunohistochemistry analysis showed that kynurenine 3-monooxygenase (KMO) and kynureninase (KYNU), enzymes converting kynurenine into 3-HAA, were downregulated in HCC cells. However, the expression of the 3-HAA degrading enzyme hydroxyanthranilate 3,4-dioxygenase (HAAO) varied in HCC cells and HCC tumors. In contrast, the indoleamine 2,3-Dioxygenase 1 (IDO1) and tryptophan 2,3-Dioxygenase (TDO2), enzyme catabolizing tryptophan into kynurenine, was upregulated in HCC cells (Fig. 2A). The immunohistochemistry analysis also showed that the KMO and KYNU expression increased in clinical HCCs (Fig. 2B). This finding was consistent with the HCC expression profile in the TCGA database (Fig. 2C). Moreover, both KMO and KYNU expression (www.gtexportal.org) are commonly downregulated in tumors originated from tissues abundantly expressing KMO ($\log2(TPM) > 2$) and KYNU ($\log2(TPM) > 3.5$). These tumors include lung, kidney, and liver carcinomas, which are top 10 tumors worldwide in terms of death. (Fig. 2D).

In addition, overexpression of KMO significantly increased the concentration of 3-HAA in HCC SMMC7721 cells, six times more than control cells, but not the hydroxykynurenine (3-HK), picolinate (PA), or quinolinate (QA) (Fig. 2E). The HAAO knockdown had similar effects on the levels of these metabolites

(Fig. 2F). These observations suggested that 3-HAA is decreased in cancer cells by upregulating KMO expression and/or downregulating HAAO.

3-HAA inhibits tumor formation by inducing apoptosis

In order to determine the effect of 3-HAA on tumor growth, exogenous 3-HAA was added to HCC cultures, and cell proliferation was assessed. Indeed, 3-HAA significantly inhibited HCC cell growth and colony formation (Figs. 3A and S3A). In contrast, the other tryptophan metabolites, kynurenine (KYN), 3-hydroxykynurenine (3-HK), and quinolinate acid (QA) did not substantially affect the growth and colony formation of HepG2 and SMMC7721 cells. Moreover, 3-HAA treatment also slowed tumor growth in a CDX (cell-derived xenograft) model and in a PDX (patient-derived xenograft) model while the same dose of kynurenine had negligible effects on xenografts' growth (Figs. S3B and 3B).

In order to verify that this effect was caused by 3-HAA and not its precursor kynurenine or 3-HK, the cellular concentrations of 3-HAA, kynurenine, and 3-HK were analyzed by LC-MS/MS in 3-HAA-treated tumor cells. Although the content of endogenous 3-HAA varied among different HCC cell lines, 3-HAA treatment increased the cellular concentration of 3-HAA, particularly in SMMC7721 and HepG2, but not kynurenine (Fig. S3C). Moreover, the cell growth was analyzed in SMMC7721 cells overexpressing KMO or knocking down HAAO enzymes. Either overexpression of KMO or knockdown of HAAO inhibited cell growth of HCC cells *in vitro* (Fig. 3C).

To determine what signal mediates 3-HAA-induced cell death, we treated tumor cells with 3-HAA and specific inhibitors to apoptosis, autophagy, and necrosis, respectively. As shown in Fig. 3D, the apoptosis inhibitor ZVAD, but not the necrosis inhibitor Nec1 or autophagy inhibitor 3-MA, restored growth of HepG2 and SMMC7721 cells following 3-HAA treatment. This effect was observed at ZVAD doses of 50 and 100 μM. The KMO overexpression increased apoptosis in HCC cells, and the apoptosis inhibitor ZVAD restored the HCC cell growth (Fig. 3E & 3F).

Moreover, the tumor formation assay showed that KMO overexpression suppressed tumor formation and tumor growth in HCC xenograft nude mice model. After inoculation of 0.5×10^6 SMMC7721 cells, the tumor formation rates within three weeks were 90% (9/10) versus 40% (4/10) in the control group and KMO overexpression group, respectively (Figs. 3G). When increasing the inoculation number of tumor cells to 1.5×10^6, the tumor volumes in KMO overexpressing group were apparently small than the control group by the end of 4 weeks (Fig. S3D). Remarkably, the Kaplan-Meier survival analysis showed that HCC patients with high KMO expression had a more prolonged disease-free survival than patients with low KMO expression (Fig. 3H). These observations suggested that 3-HAA is a negative regulator for tumor formation and tumor growth.

3-HAA induces apoptosis by upregulating DUSP6 expression

In order to determine the mechanism by which 3-HAA induces tumor cell apoptosis, RNA sequencing was used to profile gene expression in SMMC7721 or HepG2 cells after 1, 8, or 24 h treatment with 3-HAA

according to the screening strategy previously applied [7]. At all three time points after the start of 3-HAA treatment, the top 6 upregulated genes were selected (Fig. 4A). The expression of these 6 genes was individually verified by real-time PCR. Immunoblotting of the top two upregulated genes also showed elevated levels of *DUSP6* and *IGFBP1* in SMMC7721 and HepG2 cells (Fig. 4B). These results suggested that 3-HAA altered the gene expression profile of HCC cells, with *DUSP6* and *IGFBP1* as two of the most upregulated genes. However, the clinical data showed that the overall survival of HCC patients was only associated with the expression level of DUSP6 ($p < 0.05$), but not IGFBP1 ($p > 0.05$). Patients expressing a high level of DUSP6 showed a more prolonged overall survival than patients expressing a low level of DUSP6 ($p < 0.05$) (Fig. 4C), and the corrective analysis with the clinical characteristics also supported this finding (Fig. S4A), indicating that DUSP6 might mediate the 3-HAA-induced apoptosis.

To demonstrate whether DUSP6 mediating 3-HAA-induced tumor cell apoptosis, the effects of DUSP6 on HCC cell growth were first analyzed in HCC cells. *DUSP6* knockdown restored growth of HepG2 and SMMC7721 cells inhibited by 3-HAA (Figs. 4D and S4B). 3-HAA induced apoptosis to a smaller extent in DUSP6-depleted SMMC7721 cells than in the control cells, based on flow cytometry using Annexin V (Fig. 4E & S4C). DUSP6 depletion was also associated with reduced levels of cleaved caspase-3 and cleaved PARP; in the meantime, DUSP6 knockdown facilitated ERK enhancing signal on cell survival, which was consistent with the previous study [Piya, 2012] (Fig. 4F). In fact, DUSP6 knockdown restored ERK activity that had been suppressed by 3-HAA (Fig. 4F). ERK activation inhibited apoptosis via BAD/BCL2/BCL-XL signaling, consistent with the previous reports [13] [14].

Based on the previous finding that 3-HAA activates transcription factor YY1 [Shi, 2021], we speculated that 3-HAA could regulate YY1 transcription activity on *DUSP6* gene promoter. Closer analysis of the *DUSP6* promoter region using online-based prediction tools (jaspar.genereg.net and ecrbrowser.dcode.org) [15, 16] revealed a novel potential YY1 binding DNA fragment at positions − 1145 to -1134 (TCCATCCGGCTT), which was distinct from the reported consensuses binding sequence (CAANATGGCGGC) [17]. In order to determine whether YY1 regulates *DUSP6* expression by binding this novel sequence, each DNA fragment was added to a luciferase reporter gene, and YY1-driven luciferase expression was measured by its enzyme activity. Higher luciferase activity was observed with the full length or partial *DUSP6* promoter containing this novel specific sequence as well as the consensus YY1 binding sequence. Luciferase activity decreased when mutations involving this novel binding site (mut2) occurred (Fig. 4G). Moreover, the quantitative PCR analysis following chromatin immunoprecipitation of YY1 revealed that 3-HAA promoted YY1 binding to the consensus sequence of the *P53* promoter region (positive control) and the novel binding sequence in the *DUSP6* promoter region, as reflected by 3-HAA-induced YY1 enrichment (Figs. 4H & S4D). The TUNEL assay demonstrated that 3-HAA-induced apoptosis was also reduced in SMMC7721 cells depleted of YY1, overexpression of DUSP6 restored the apoptosis suppressed by YY1 depletion (Fig. 4I), suggesting DUSP6 mediates 3-HAA-induced HCC apoptosis.

3-HAA synergizes with IDO1 inhibitor on HCC growth

To further evaluate the potential application of 3-HAA in clinics, the various HCC mouse models were implemented in this study. As shown in Fig. 5A, *DUSP6* knockdown reversed 3-HAA-mediated suppression of tumor growth in SMMC7721 xenografts, of which the SMMC7721 cells were depleted of DUSP6 by shRNAs before inoculation. More impressively, 3-HAA treatment reduced the tumor numbers and prolonged the survival in a transposon HCC mouse model. DUSP6 depletion promoted tumor formation and shorten mice survival, and 3-HAA treatment had little effect on tumor formation and mice survival after DUSP6 knockdown (Fig. 5B).

Most importantly, 3-HAA synergized with IDO1 inhibitor Epacadostat to suppress HCC xenograft growth in an immune-competent mouse model (Fig. 5C). In the meantime, the combination of 3-HAA with IDO1 inhibitor Epacadostat also inhibited the genetic HCC tumor growth and prolonged the survival of mice bearing transposon-induced HCCs (Fig. 5D).

In order to evaluate the stability of 3-HAA *in vivo*, the concentration of 3-HAA was analyzed at the time course of administration in the plasma of mice. As shown in Fig. S5A, the half-life of 3-HAA was 3.89 hours in the serum of mice. The concentration of 3-HAA reached 71.3 μmol per gram in tumors post seven days of treatment. The seven days' administration of 3-HAA at the dose of 100 mg/kg.day did not induce apoptosis of naïve T lymphocytes in the spleen (Fig. S5B). These results highlighted the promise of 3-HAA as a potential HCC therapy.

Discussion

Tryptophan metabolism plays a critical role in development and tumor progression. It not only provides critical intermediates for anabolism but also regulates cell signaling. IDO converts tryptophan into kynurenine, which is a well-known functional metabolite of tryptophan and could be further catabolized to 3-HAA. Kynurenine binds AHR to induce immune suppression (tolerance), which is associated with successful embryo implantation but also with poor prognosis in various malignancies. The inhibition of IDO1/2 suppressed tumor formation in animal models but failed in stage III of clinical trials. This is probably due to the expression of the other kynurenine generating enzyme TDO, which may not be suppressed by the IDO inhibitor. However, the 3-HAA treatment reverses the tumor-promoting effect of kynurenine and significantly improves the efficacy of IDO1/2 inhibitors on HCC xenografts, suggesting 3-HAA as a negative feedback regulator reverses the tumor cell-hijacked tryptophan metabolism.

The 3-HAA exerted anti-inflammatory and neuroprotective effects by selectively inducing the apoptosis of activated T cells or suppressing microglia/astrocytes that expressing cytokines and chemokines [11, 12]. The 3-HAA induced the expression of cytoprotective enzyme hemeoxygenase-1 in astrocytes and microglia; the latter is an enzyme with proven anti-inflammatory and cytoprotective activities [18, 19]. The 3-HAA-induced apoptosis of activated T lymphocytes was linked to oxidative stress and induction of caspases [20, 21]. These results indicated that 3-HAA has a distinct biological function in a different type of cells. However, the biological function of 3-HAA largely remained unclear.

In this study, we report that 3-HAA decreases in HCC cells and HCC tissues due to the downregulation of KMO and KYNU enzymes as well as the upregulation of the HAAO enzyme. The excessive kynurenine generated from tryptophan, in return, regulates these enzyme expressions by autocrine or paracrine of HCC cells [22, 23]. Also, we observe that the sensitivity of HCC cell to 3-HAA, to some extent, are correlated with the cellular 3-HAA concentration after 3-HAA treatment. However, the increase of intracellular 3-HAA concentration post-3-HAA treatment may not completely associate with expression levels of KMO, KYNU, or HAAO enzymes in HCC cells, since the 3-HAA transporters and drug-resistant genes may also involve in the regulation of HCC sensitivity to 3-HAA. This observation suggests that the heterogeneity of tryptophan metabolism in HCC cells may determine their sensitivity to 3-HAA.

Conclusion

In brief, both the increase of 3-HAA and upregulation of 3-HAA synthetic enzyme KMO suppresses HCC growth in the PDX and transposon-induced HCC mouse model by inducing apoptosis of HCC cell, suggesting the 3-HAA metabolic pathway is important to HCC growth and downregulation of 3-HAA appears to be essential for HCC growth. Exogenous 3-HAA or KMO overexpression induces HCC cell apoptosis, sequentially reduces the formation and growth of HCC; moreover, the 3-HAA treatment improves the efficacy of IDO1/2 inhibitors on HCC growth, suggesting its potential use in HCC therapy.

Abbreviations

AHR
aryl hydrocarbon receptor
3-HAA
3-hydroxyanthranilic acid
DUSP
dual-specificity phosphatase 6
HCC
hepatocellular carcinoma
TDO2
2,3-dioxygenase 1/2
IDO1/2
tryptophan 2,3-dioxygenase
PBS
phosphate-buffered saline
BCA
bicinchoninic acid
PFA
paraformaldehyde
HDT

hydrodynamic transfection
LC-MS/MS
liquid chromatography-tandem mass spectrometry
GC-MS
gas chromatography-mass spectrometry
3-HK
3-hydroxykynurenine
KMO
kynurenine 3-monooxygenase
KYNU
kynureninase
HAAO
hydroxyanthranilate 3,4-dioxygenase
IDO1
indoleamine 2,3-Dioxygenase 1
TDO2
tryptophan 2,3-Dioxygenase
3- HK
4- hydroxykynurenine
PA
picolinate
QA
quinolinate
KYN
kynurenine
PDX
patient-derived xenograft

Declarations

Ethics approval and consent to participate

This study received animal ethics board approval at the Shanghai Jiao Tong University School of Medicine.

Consent for publication

Not applicable.

Availability of data and material

The data used to support the findings of this study are available from the corresponding author upon request.

Competing interests

The authors declare that they have no competing interests.

Funding

This study was supported by grants from the Ministry of Science and Technology of the People's Republic of China (2018YFC1313205), the Shanghai Committee of Science and Technology (11DZ2260200) (20JC1410100) and the National Natural Science Foundation of China (81572300) (81872342) to Dr. Mi.

Authors' contributions

Z.S., G.G. performed most of the experiments; X.G. performed metabolites mass-spectrometry analysis; J.M., F.C. initiated the project, led the project team, designed experiments, analyzed results, and wrote the paper with input from all authors.

Acknowledgements

We thank Profs. Shimin Zhao (Fudan University School of Biology) and Weiwei Yang (Shanghai Institute of Biochemistry and Cell Biology, Chinese Academy of Science) for useful discussions.

References

1. Schrocksnadel K, Wirleitner B, Winkler C, Fuchs D. Monitoring tryptophan metabolism in chronic immune activation. Clin Chim Acta. 2006;364:82–90.
2. Chen Y, Guillemin GJ. Kynurenine pathway metabolites in humans: disease and healthy States. International journal of tryptophan research: IJTR. 2009;2:1–19.
3. Terai M, Londin E, Rochani A, Link E, Lam B, Kaushal G, Bhushan A, Orloff M, Sato T: **Expression of Tryptophan 2,3-Dioxygenase in Metastatic Uveal Melanoma**. *Cancers (Basel)* 2020, **12**.
4. Li S, Weng J, Song F, Li L, Xiao C, Yang W, Xu J. Circular RNA circZNF566 promotes hepatocellular carcinoma progression by sponging miR-4738-3p and regulating TDO2 expression. Cell Death Dis. 2020;11:452.
5. Sadik A, Somarribas Patterson LF, Ozturk S, Mohapatra SR, Panitz V, Secker PF, Pfander P, Loth S, Salem H, Prentzell MT, et al. IL4I1 Is a Metabolic Immune Checkpoint that Activates the AHR and Promotes Tumor Progression. Cell. 2020;182:1252–70 e1234.
6. Lercher A, Popa AM, Viczenczova C, Kosack L, Klavins K, Agerer B, Opitz CA, Lanz TV, Platten M, Bergthaler A. Hepatocyte-intrinsic type I interferon signaling reprograms metabolism and reveals a

novel compensatory mechanism of the tryptophan-kynurenine pathway in viral hepatitis. PLoS Pathog. 2020;16:e1008973.

7. Opitz CA, Litzenburger UM, Sahm F, Ott M, Tritschler I, Trump S, Schumacher T, Jestaedt L, Schrenk D, Weller M, et al. An endogenous tumour-promoting ligand of the human aryl hydrocarbon receptor. Nature. 2011;478:197–203.
8. Sharma MD, Baban B, Chandler P, Hou DY, Singh N, Yagita H, Azuma M, Blazar BR, Mellor AL, Munn DH. Plasmacytoid dendritic cells from mouse tumor-draining lymph nodes directly activate mature Tregs via indoleamine 2,3-dioxygenase. J Clin Invest. 2007;117:2570–82.
9. Li Y, Innocentin S, Withers DR, Roberts NA, Gallagher AR, Grigorieva EF, Wilhelm C, Veldhoen M. Exogenous stimuli maintain intraepithelial lymphocytes via aryl hydrocarbon receptor activation. Cell. 2011;147:629–40.
10. Schwarcz R, Bruno JP, Muchowski PJ, Wu HQ. Kynurenines in the mammalian brain: when physiology meets pathology. Nature reviews Neuroscience. 2012;13:465–77.
11. Krause D, Suh HS, Tarassishin L, Cui QL, Durafourt BA, Choi N, Bauman A, Cosenza-Nashat M, Antel JP, Zhao ML, Lee SC. The tryptophan metabolite 3-hydroxyanthranilic acid plays anti-inflammatory and neuroprotective roles during inflammation: role of hemeoxygenase-1. Am J Pathol. 2011;179:1360–72.
12. Lee SM, Lee YS, Choi JH, Park SG, Choi IW, Joo YD, Lee WS, Lee JN, Choi I, Seo SK. Tryptophan metabolite 3-hydroxyanthranilic acid selectively induces activated T cell death via intracellular GSH depletion. Immunology letters. 2010;132:53–60.
13. Cagnol S, Chambard JC. ERK and cell death: mechanisms of ERK-induced cell death–apoptosis, autophagy and senescence. FEBS J. 2010;277:2–21.
14. Piya S, Kim JY, Bae J, Seol DW, Moon AR, Kim TH. DUSP6 is a novel transcriptional target of p53 and regulates p53-mediated apoptosis by modulating expression levels of Bcl-2 family proteins. FEBS Lett. 2012;586:4233–40.
15. Khan A, Fornes O, Stigliani A, Gheorghe M, Castro-Mondragon JA, van der Lee R, Bessy A, Cheneby J, Kulkarni SR, Tan G, et al. JASPAR 2018: update of the open-access database of transcription factor binding profiles and its web framework. Nucleic Acids Res. 2018;46:D1284.
16. Khan A, Fornes O, Stigliani A, Gheorghe M, Castro-Mondragon JA, van der Lee R, Bessy A, Cheneby J, Kulkarni SR, Tan G, et al. JASPAR 2018: update of the open-access database of transcription factor binding profiles and its web framework. Nucleic Acids Res. 2018;46:D260–6.
17. Kim J, Kim J. YY1's longer DNA-binding motifs. Genomics. 2009;93:152–8.
18. Brusko TM, Wasserfall CH, Agarwal A, Kapturczak MH, Atkinson MA. An integral role for heme oxygenase-1 and carbon monoxide in maintaining peripheral tolerance by CD4 + CD25 + regulatory T cells. J Immunol. 2005;174:5181–6.
19. Ryter SW, Choi AM. Heme oxygenase-1/carbon monoxide: from metabolism to molecular therapy. Am J Respir Cell Mol Biol. 2009;41:251–60.

20. Hiramatsu R, Hara T, Akimoto H, Takikawa O, Kawabe T, Isobe K, Nagase F. Cinnabarinic acid generated from 3-hydroxyanthranilic acid strongly induces apoptosis in thymocytes through the generation of reactive oxygen species and the induction of caspase. Journal of cellular biochemistry. 2008;103:42–53.
21. Hayashi T, Mo JH, Gong X, Rossetto C, Jang A, Beck L, Elliott GI, Kufareva I, Abagyan R, Broide DH, et al. 3-Hydroxyanthranilic acid inhibits PDK1 activation and suppresses experimental asthma by inducing T cell apoptosis. Proc Natl Acad Sci U S A. 2007;104:18619–24.
22. Liu Y, Liang X, Dong W, Fang Y, Lv J, Zhang T, Fiskesund R, Xie J, Liu J, Yin X, et al. Tumor-Repopulating Cells Induce PD-1 Expression in CD8(+) T Cells by Transferring Kynurenine and AhR Activation. Cancer Cell. 2018;33:480–94 e487.
23. Liu Y, Liang X, Yin X, Lv J, Tang K, Ma J, Ji T, Zhang H, Dong W, Jin X, et al. Blockade of IDO-kynurenine-AhR metabolic circuitry abrogates IFN-gamma-induced immunologic dormancy of tumor-repopulating cells. Nat Commun. 2017;8:15207.
24. Huynh H, Soo KC, Chow PK, Panasci L, Tran E. Xenografts of human hepatocellular carcinoma: a useful model for testing drugs. Clinical cancer research: an official journal of the American Association for Cancer Research. 2006;12:4306–14.
25. Chen X, Calvisi DF. Hydrodynamic transfection for generation of novel mouse models for liver cancer research. Am J Pathol. 2014;184:912–23.
26. Wang C, Vegna S, Jin H, Benedict B, Lieftink C, Ramirez C, de Oliveira RL, Morris B, Gadiot J, Wang W, et al. Inducing and exploiting vulnerabilities for the treatment of liver cancer. Nature. 2019;574:268–72.
27. Sun X, Wang SC, Wei Y, Luo X, Jia Y, Li L, Gopal P, Zhu M, Nassour I, Chuang JC, et al. Arid1a Has Context-Dependent Oncogenic and Tumor Suppressor Functions in Liver Cancer. Cancer Cell. 2018;33:151–2.

Figures

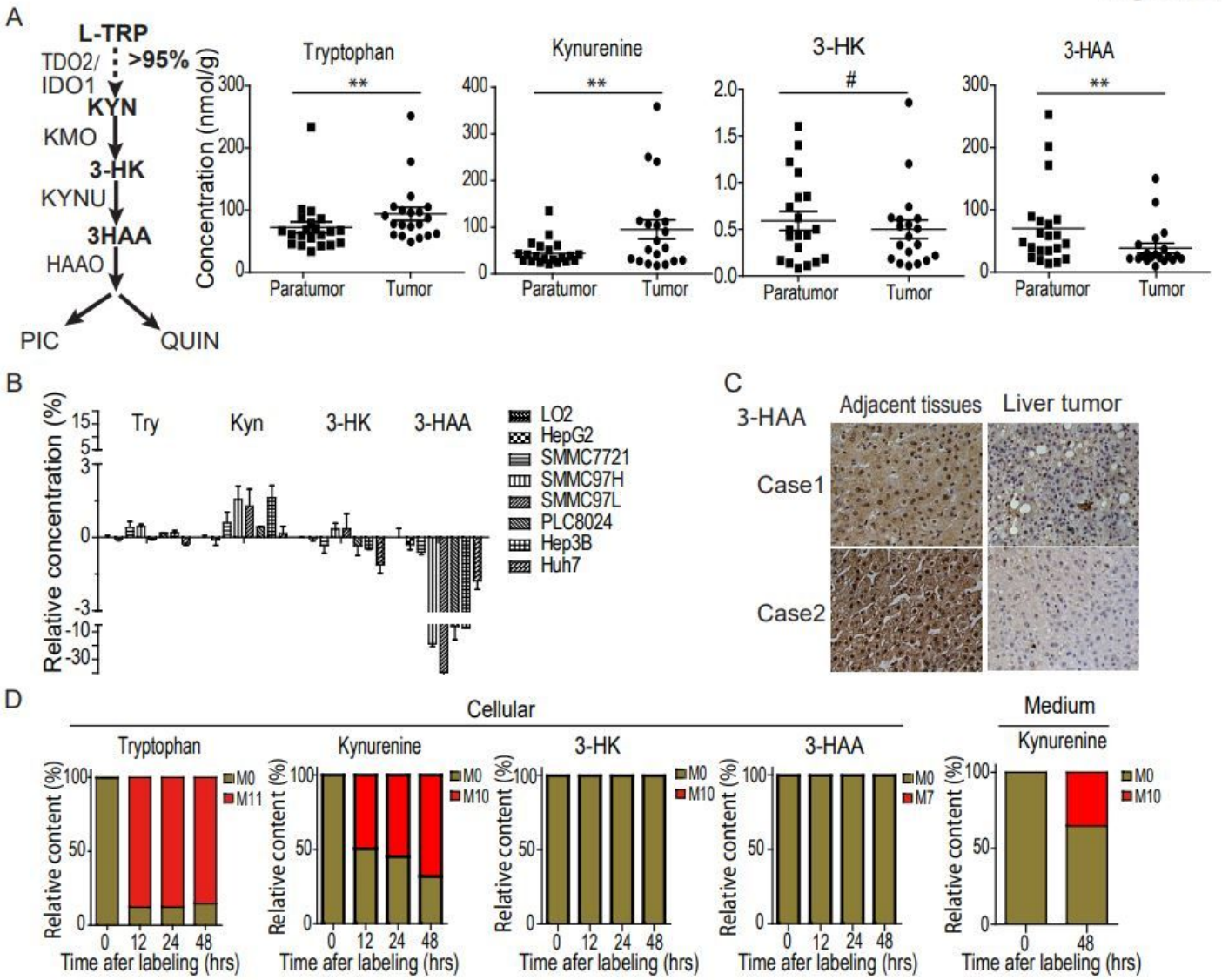

Figure 1

3-HAA is decreased in tumor cells A. Quantitative analysis of tryptophan metabolites by LC-MS/MS and GC-MS in HCC and the corresponding paratumor tissues. **: P<0.01. B. Quantitative analysis of tryptophan metabolites by LC-MS/MS and GC-MS in normal hepatic cells and HCC cells. C. The immunohistochemistry staining of 3-HAA on HCC samples. D. Metabolic flux analysis of tryptophan metabolites in SMMC-7721 and HepG2 cells. L-Tryptophan was completely 13C-labelled. The content of tryptophan catabolites in cells and medium was assessed using LC-MS/MS. The M0 stands for no carbon in tryptophan was 13C-labelled, M11 stands for all 11 carbon in tryptophan were 13C-labelled.

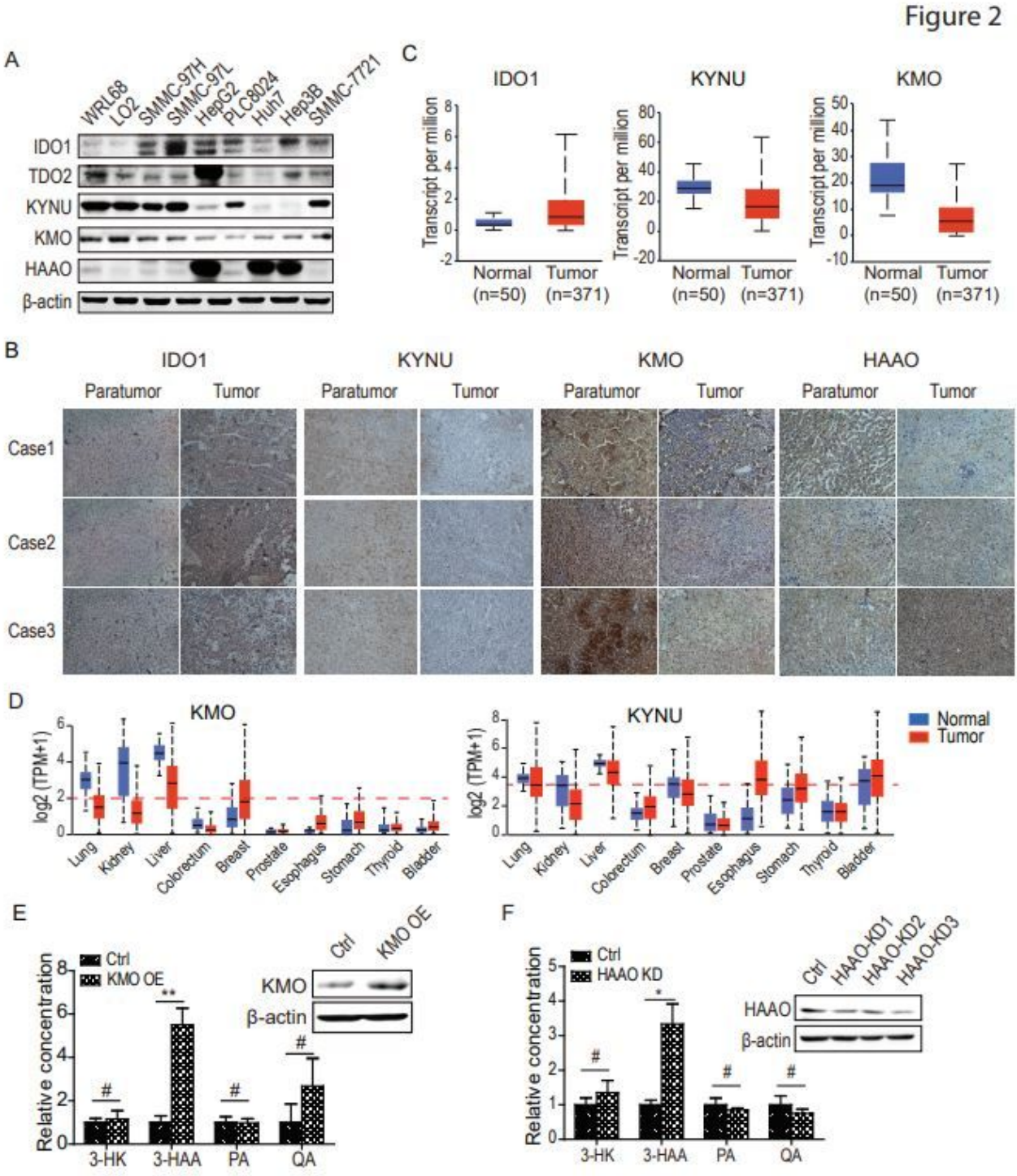

Figure 2

3-HAA is decreased by downregulation of its upstream catabolizing enzyme KMO A. Expression analysis of metabolic enzymes involved in 3-HAA generation. B. The immunohistochemistry staining of KYNU, KMO, IDO and HAAO on HCC samples. C. The expression profile of KYNU, KMO, and IDO1 in the HCC samples by RNA-seq. D. The expression profile of KMO and KYNU in top 10 tumors in terms of death and the corresponding normal tissues. E. The effect of KMO overexpression on the concentration of

endogenous 3-HAA and tryptophan catabolites in SMMC7721 cells. **: P<0.01. F. The quantitative analysis of 3-HK, 3-HAA, PA, and QA in SMMC7721 cells depleted of HAAO.

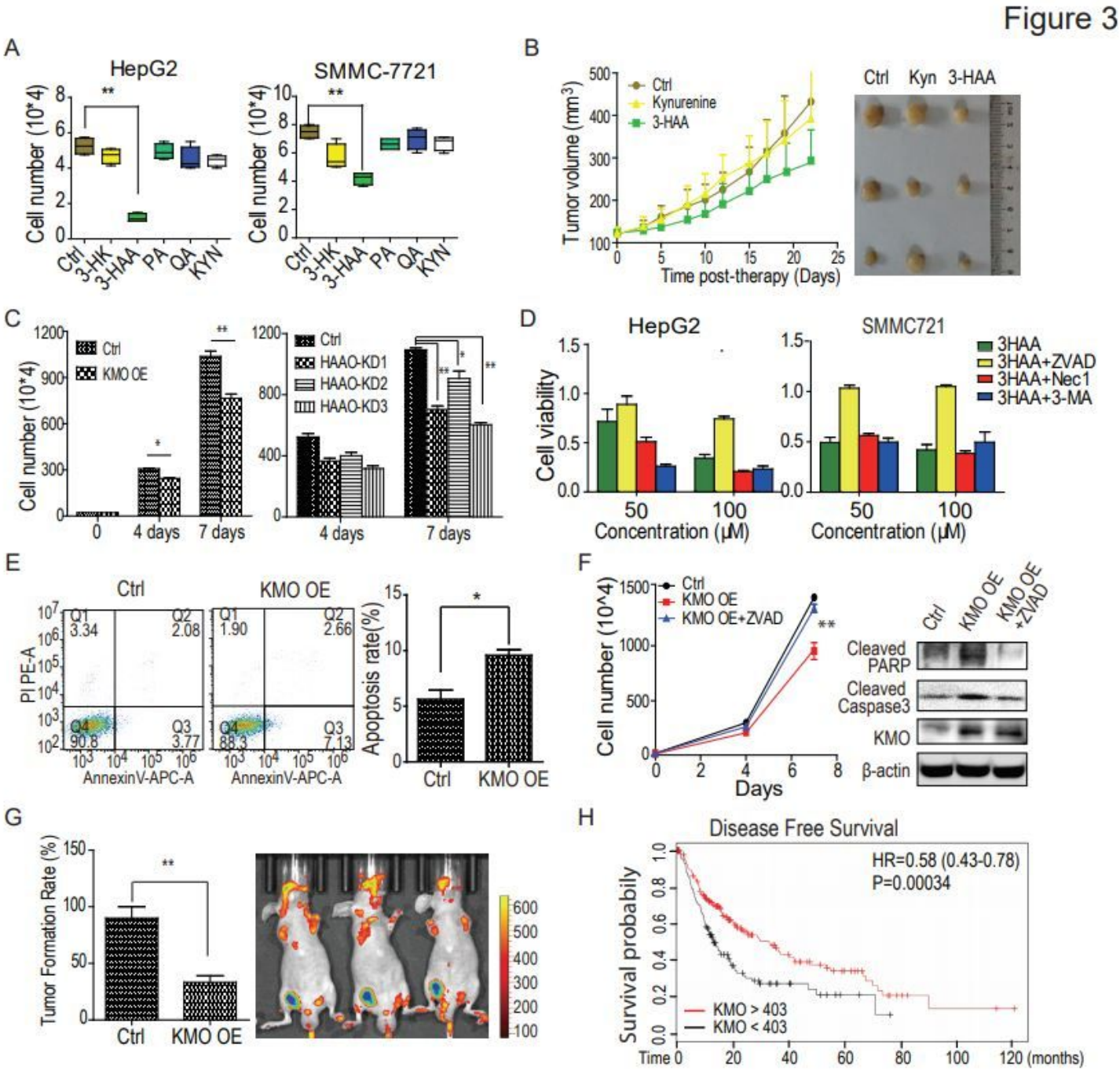

Figure 3

3-HAA inhibits tumor formation by inducing apoptosis A. Analysis of the growth of HCC cells treated for four days with one of five tryptophan metabolites (100 μM). **: P<0.01. B. 3-HAA but not kynurenine slowed the xenograft growth of PDX HCCs. C. The effect of HAAO and KMO on the cell growth of SMMC7721 cells. The KMO and HAAO was overexpressed or knocked down in SMMC7721 cells, separately. D. The effects of three types of inhibitors on 3-HAA-induced HCC cell death. ZVAD: apoptosis

inhibitor (20 μM); Nec1: necrosis inhibitor (100 μM); 3-MA: autophagy inhibitor (5 mM). The dose of 3-HAA was 100 μM. Cells were treated for four days. *: P<0.05, **: P<0.01. E. The effect of KMO overexpression on apoptosis of SMMC7721 cells. *: P<0.05. F. The influence of KMO overexpression on cell growth and apoptotic signal of HCC cells. The KMO was over-expressed in SMMC-7721. **: $p < 0.01$. The dose of 3-HAA and ZVAD was 100 μM and 20 μM, respectively. G. The influence of KMO overexpression on tumor formation of HCC cells and the representative living image of HCC xenografts expressing KMO. The KMO was overexpressed in SMMC 7721 (n=10). The **: $p < 0.01$. H. The K_M plot analysis of KMO expression with the disease-free survival of HCC patients. The patients were divided by the median of KMO expression value.

Figure 4

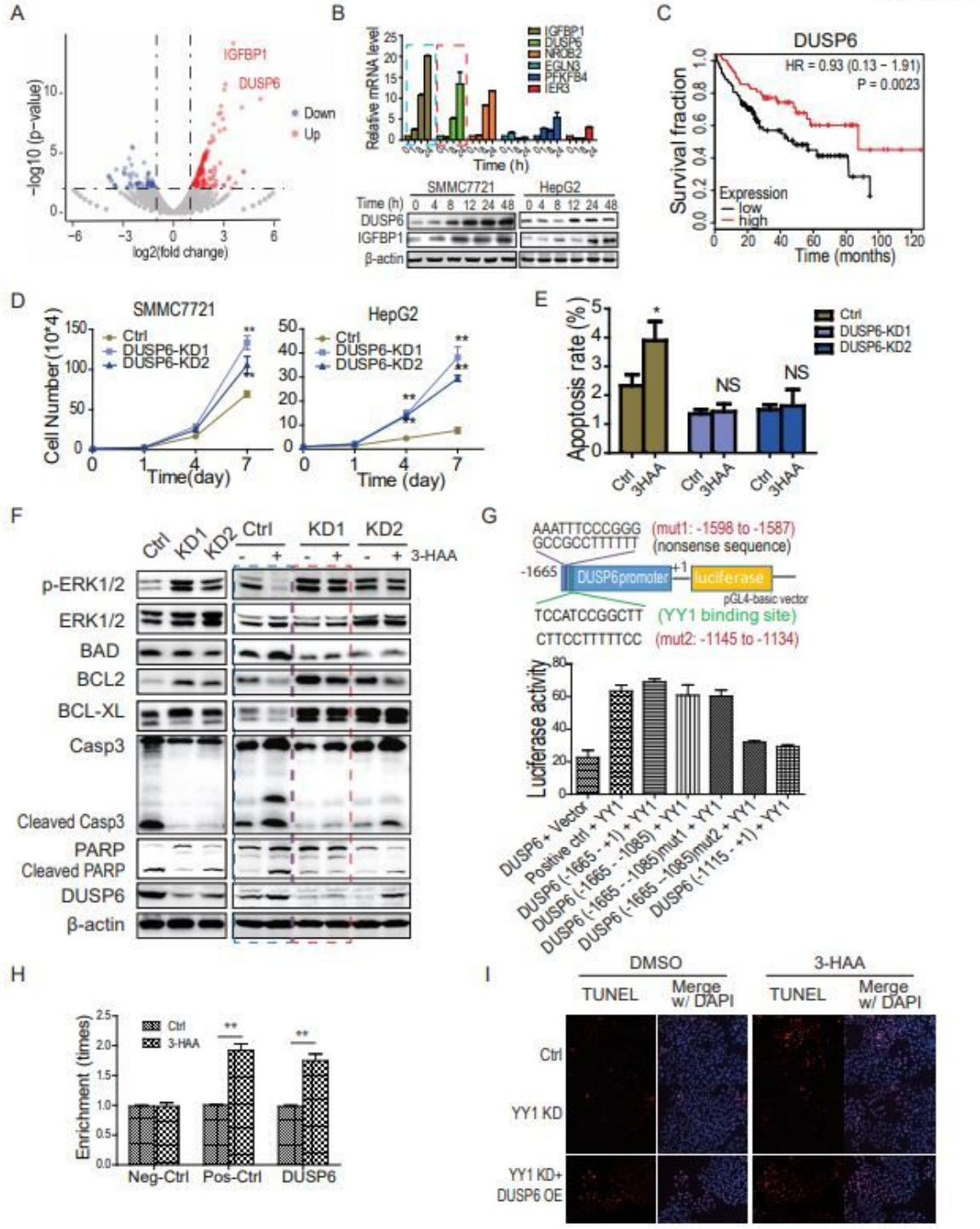

Figure 4

3-HAA induces apoptosis by upregulating DUSP6 A. The volcano map of the top consistently upregulated genes in SMMC7721, and HepG2. Deep sequencing was used to profile gene expression in HCC SMMC7721, Hep3B, and SMMC97H cells. HCC cells were treated with 100 μM 3-HAA for 1, 8, or 24 h. B. Top consistently upregulated genes were individually verified using quantitative PCR and immunoblotting. C. DUSP6 expression correlated with overall survival of HCC patients, as analyzed by the

K-M plotter. The total patient number was 415. The HCC patients were divided into two groups by the median value of KMO expression. D. Effects of DUSP6 knockdown on the growth of HCC cells. Cells were treated with 100 μM 3-HAA for the indicated time. DUSP6 was stably knocked down in SMMC7721 cells using lentivirus-generated shRNA. **: P<0.01. E. Effects of DUSP6 knockdown on HCC cell apoptosis. SMMC7721 cells were treated with 100 μM of 3-HAA for 12 h, stained for Annexin V, and analyzed by flow cytometry. *: P<0.05. F. Effects of DUSP6 knockdown on 3-HAA-activated apoptotic signaling. SMMC7721 cells depleted of DUSP6 were treated with 100 μM 3-HAA for 24 h. G. Transcription activity of YY1 on the DUSP6 promoter, as determined in a luciferase reporter assay. The schematic depicts the plasmid encoding luciferase under the control of the DUSP6 promoter, which was truncated or mutated as indicated. H. The ChIP-PCR analysis. The positive control (PC) is TP53. I. The apoptosis analysis by TUNEL assay in SMMC7721 cells depleted of YY1 and/or overexpressing DUSP6.

Figure 5

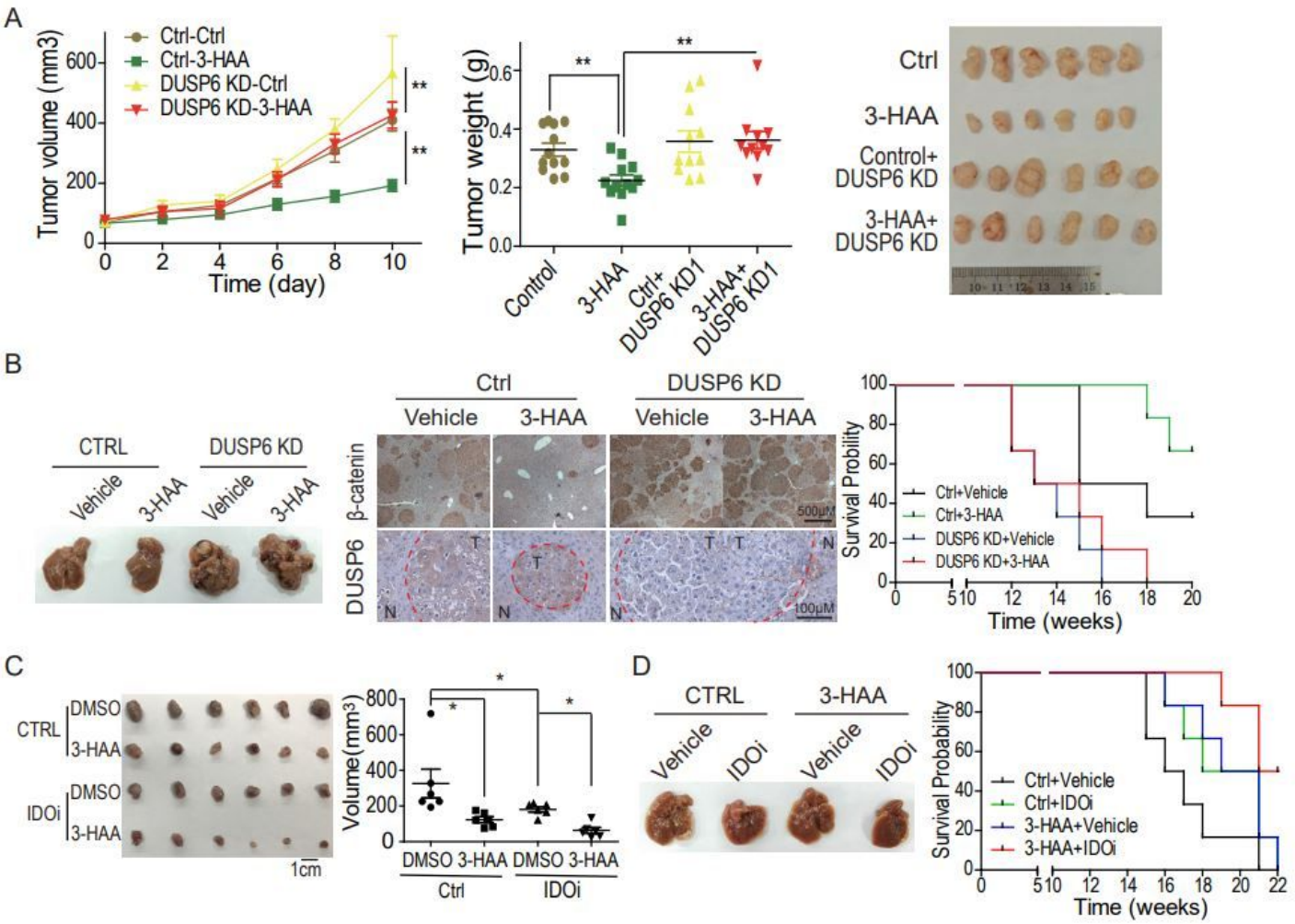

Figure 5

3-HAA synergizes with IDO1 inhibitor on HCC growth A. DUSP6 knockdown recovered 3-HAA-suppressed xenograft growth. Animals were treated with 3-HAA (100 mg/kg•day) for seven days, then sacrificed on

day 10. SMMC7721 cells were subcutaneously injected into mice. The middle graph shows xenograft weights in different groups. Photographs on the right show representative tumors in different groups (n=6). **: P<0.01. B. DUSP6 knockdown restored 3-HAA-reduced tumor numbers and shortened the survival of mice bearing transposon HCCs. The genetic transposon HCC mouse model was established as described in the section of methods and materials (n=6). C. 3-HAA synergizes with IDO1 inhibitor Epacadostat to suppress HCC xenograft growth. The mouse liver cancer Hep1-6 cells (1 × 106) were inoculated into immune-competent C57BL/6 mice (n=6). *: P<0.05. D. 3-HAA synergizes with IDO1 inhibitor Epacadostat to prolong the survival of mice bearing transposon HCCs. The dose of both 3-HAA and Epacadostat (IDO1 inhibitor) was 100 mg/kg.day, respectively. Note: The mouse xenografts were generated by the inoculation of 1.5 x 10^6 of SMMC7721 cells into the armpit of the rear limb. The 3-HAA (100 mg/kg.day) was administered by intraperitoneal injection for seven days. Tumor volumes are presented as mean ± SD (*: P < 0.05; **: P < 0.01.). Photographs show representative xenografts in different groups.

Supplementary Files

This is a list of supplementary files associated with this preprint. Click to download.

- SuppFigures.pdf